

Open Research Online

The Open University's repository of research publications
and other research outputs

Numerical description of discharge characteristics of the plasma needle

Journal Item

How to cite:

Brok, W. J. M.; Bowden, M. D.; van Dijk, J.; van der Mullen, J. J. A. M. and Kroesen, G. M. W. (2005). Numerical description of discharge characteristics of the plasma needle. *Journal of Applied Physics*, 98(1), article no. 013302 (8 pages).

For guidance on citations see [FAQs](#).

© 2005 American Institute of Physics

Version: Version of Record

Link(s) to article on publisher's website:
<http://dx.doi.org/doi:10.1063/1.1944218>

Copyright and Moral Rights for the articles on this site are retained by the individual authors and/or other copyright owners. For more information on Open Research Online's data [policy](#) on reuse of materials please consult the policies page.

oro.open.ac.uk

Numerical description of discharge characteristics of the plasma needle

W. J. M. Brok,^{a)} M. D. Bowden, J. van Dijk, J. J. A. M. van der Mullen, and G. M. W. Kroesen

Department of Applied Physics, Eindhoven University of Technology, P.O. Box 513, 5600 MB, Eindhoven, The Netherlands

(Received 14 December 2004; accepted 6 May 2005; published online 7 July 2005)

The plasma needle is a small atmospheric, nonthermal, radio-frequency discharge, generated at the tip of a needle, which can be used for localized disinfection of biological tissues. Although several experiments have characterized various qualities of the plasma needle, discharge characteristics and electrical properties are still not well known. In order to provide initial estimates on electrical properties and quantities such as particle densities, we employed a two-dimensional, time-dependent fluid model to describe the plasma needle. In this model the balance equation is solved in the drift-diffusion approach for various species and the electron energy, as well as Poisson's equation. We found that the plasma production occurs in the sheath region and results in a steady flux of reactive species outwards. Even at small ($<0.1\%$) admixtures of N_2 to the He background, N_2^+ is the dominant ion. The electron density is typically 10^{11} cm^{-3} and the dissipated power is in the order of 10 mW. These results are consistent with the experimental data available and can give direction to the practical development of the plasma needle. © 2005 American Institute of Physics. [DOI: 10.1063/1.1944218]

I. INTRODUCTION

Nonthermal atmospheric plasmas have recently attracted much attention due to their applicability in biomedical technology.^{1,2} The main characteristic of such a plasma is that the gas temperature stays low, typically not much more than a biologically compatible 310 K. The electron temperature, however, is several ten thousands kelvin and this leads to the production of many reactive species such as excited molecules, radicals, and ions. These species can react with molecules in the tissue and thereby accomplish the disinfective purpose of the device.

One of the promising nonthermal plasma devices is the recently developed plasma needle.¹ In several experimental studies, Stoffels and co-workers^{3,4} have shown it to be capable of locally killing cells and loosening them from their substrate for removal. This allows malignant cells to be disposed of in an orderly fashion, diminishing the risk of infections and damage to nearby benign cells: the cell membrane stayed intact and thus kept the potentially harmful content of the cell contained.

The active medium of the plasma needle is a small ($\sim 1 \text{ mm}$) atmospheric, nonthermal radio-frequency (rf) plasma, generated at the tip of a metal wire (see Fig. 1). The needle itself can be held as one holds a pen and is connected to a gas cylinder and a power supply via a small tube and a wire. This arrangement makes it practical as a tool in future applications such as dentistry and microsurgery. However, before it can be considered safe and suitable for these medical applications, the plasma and its properties need to be investigated further: the interactions between the species and the interplay of the charged particles with the electric fields

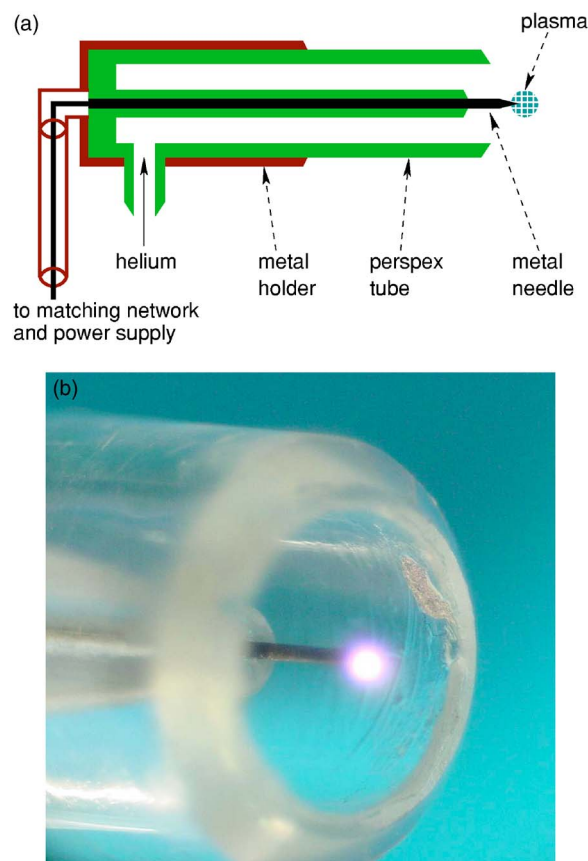


FIG. 1. (Color online) Top figure: a schematic drawing of the plasma needle. Bottom figure: a picture taken of the tip of the needle in operation. The needle itself is a sharpened metal wire with a diameter of 0.3 mm. The perspex tube around it has an inner diameter of 5 mm and serves to direct the flow of helium along the needle. The needle is isolated for a large part in order to prevent a discharge from forming within the tube. Refer to Ref. 17 for more details concerning the device.

^{a)}Electronic mail: j.j.a.m.v.d.mullen@tue.nl

make the plasma a complex nonequilibrium system, which can be improved more efficiently if a theoretical description is available.

Unlike the plasma needle, theoretical descriptions do exist for other types of atmospheric, nonthermal plasmas (see, e.g., Refs. 5–7). These devices are in a similar manner employed for disinfection and surface treatment of materials that do not react well to vacuum or high temperatures. However, their active region is larger and does not allow for very localized treatments of surfaces.

The aim of the present research was to provide an initial numerical description for the plasma needle. This description provided estimates of important plasma properties and insight in the physical processes that determine those properties. Among these properties are species densities and the production rates for the various chemically active species, as a function of experimental settings such as the applied voltage. With these insights the plasma can be optimized for its purpose.

We used a versatile, time-dependent, two-dimensional fluid model, earlier applied in the context of plasma display panels⁸ and the ignition of compact fluorescent lamps.⁹ This model included the relatively terse, but appropriate set of reactions taken from dielectric barrier discharge literature,⁶ a cylindrically symmetric geometrical representation of the needle and a simplified description of the circuit that drives the discharge.

In this paper we present our numerical approximation of the needle, the results of the calculations done with this model, and a discussion of these results.

II. THE MODEL

In this section, the model we used is described in its various aspects: the equations that were solved, the data on the various species and reactions, and finally the geometry of the needle and its surroundings and the electrical circuit that drives the discharge.

A. Model description

The numerical model that was employed is described fully in Ref. 9 and references therein. Briefly, it is a time-dependent, two-dimensional fluid model: for a number of species (electrons, excited states, and ions) the particle density balance equation is solved in the drift-diffusion approach

$$\frac{\partial n_p}{\partial t} + \nabla \cdot \Gamma_p = S_p, \quad (1)$$

with

$$\Gamma_p = \pm \mu_p E n_p - D_p \nabla n_p, \quad (2)$$

where n_p the density of species p , S_p the source of the species due to reactions, μ_p and D_p the species' mobility and diffusion coefficient, respectively, and E the electric field.

The density and temperature of the neutral background gas were assumed to be constant in time and uniform in space. The electron energy was determined by solving the electron energy balance equation in a form similar to the equations above, with an extra source term containing the

TABLE I. The list of species for which the balance equation was solved, including references to the literature sources of the various coefficients.

Species	Diffusion coeff.	Mobility	Sec. emiss. coeff.
e	a	b, c	
He^*	d		b
He^+	a	e	b
He_2^*	d		
He_2^+	a	e	b
N_2^+	a	e	b

^aObtained from the mobility using the Einstein relation.

^bReference 13.

^cReference 11.

^dReference 14.

^eReference 15.

electric field. Poisson's equation was solved in order to account for the influence of charged species on the electric field.

A possible deviation from a Maxwellian energy spectrum for the electrons was taken into account by constructing a set of tables for transport coefficients and reaction-rate coefficients as functions of the mean electron energy. These tables were obtained from an external Boltzmann solver,¹¹ in which it was assumed that the density of the neutral ground-state background gas was stationary and uniform, as in the fluid model itself. This assumption implies that the densities of the excited and charged species stay small compared to the density of the background gas, so that pressure gradients can be neglected.

The boundary conditions to the various balance equations are listed completely in Ref. 9. They included deexcitation of excited species and neutralization of ions, as well as secondary electron emission.

B. Species and reactions

Table I lists the set of species for which the balance equations were solved and Table II gives the complete set of reactions that was used in the model. For these sets we fol-

TABLE II. The set of reactions treated in the model, with the references to the literature from which the reaction-rate coefficients were obtained.

No.	Reaction	Rate coefficient	Ref.
0	$\text{He} + e \rightarrow \text{He} + e$	from Boltzmann solver	11
1	$\text{He} + e \rightarrow \text{He}^* + e$	from Boltzmann solver	11
2	$\text{He} + e \rightarrow \text{He}^+ + 2e$	from Boltzmann solver	11
3	$\text{He}^* + e \rightarrow \text{He}^+ + 2e$	from Boltzmann solver	11 and 16
4	$\text{He}^* + 2\text{He} \rightarrow \text{He}_2^* + \text{He}$	$2.0 \times 10^{-34} \text{ cm}^3 \text{ s}^{-1}$	6
5	$\text{He}^+ + 2\text{He} \rightarrow \text{He}_2^+ + \text{He}$	$1.1 \times 10^{-31} \text{ cm}^3 \text{ s}^{-1}$	6
6	$\text{He}_2^* + M \rightarrow 2\text{He} + M$	10^4 s^{-1}	6 ^a
7	$2\text{He}^* \rightarrow \text{He}_2^* + e$	$1.5 \times 10^{-9} \text{ cm}^3 \text{ s}^{-1}$	6
8	$2\text{He}_2^* \rightarrow \text{He}_2^+ + 2\text{He} + e$	$1.5 \times 10^{-9} \text{ cm}^3 \text{ s}^{-1}$	6
9	$\text{He}_2^* + e \rightarrow \text{He}^* + \text{He}$	$8.9 \times 10^{-9} (T_e/T_g)^{-1.5} \text{ cm}^3 \text{ s}^{-1}$	6
10	$\text{He}^* + \text{N}_2 \rightarrow \text{N}_2^* + \text{He} + e$	$5.0 \times 10^{-11} \text{ cm}^3 \text{ s}^{-1}$	6
11	$\text{He}_2^* + \text{N}_2 \rightarrow \text{N}_2^+ + 2\text{He} + e$	$3.0 \times 10^{-11} \text{ cm}^3 \text{ s}^{-1}$	6
12	$\text{He}_2^+ + \text{N}_2 \rightarrow \text{N}_2^+ + \text{He}_2^*$	$1.4 \times 10^{-9} \text{ cm}^3 \text{ s}^{-1}$	6
13	$\text{N}_2^+ + e \rightarrow 2\text{N} \rightarrow \text{N}_2$	$4.8 \times 10^{-7} (T_e/T_g)^{-0.5} \text{ cm}^3 \text{ s}^{-1}$	6 ^b

^aThe symbol M represents an arbitrary heavy collision partner.

^bThe intermediate reaction products were not described in the model.

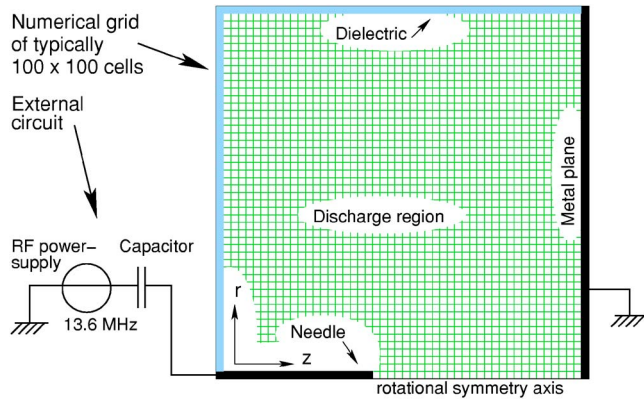


FIG. 2. (Color online) A schematic diagram of the numerical grid and the circuit driving the discharge. The discharge region was bounded on the right by a metal plane and on the left and in radial direction by a dielectric. The needle itself was located on the axis of the system. The metal plane was connected to earth and the needle to a rf power supply via a capacitor.

lowed the approach by Golubovskii *et al.*⁶ One important assumption made in their data set was that only a few excited states are needed in order to describe the discharge behavior. For the helium atom, this means that only the metastable levels were included, lumped together in one state, denoted by He^* . For the helium molecular system, the various excimer levels were assumed to decay into the $\text{He}_2(a^3\Sigma_u^+)$ state (denoted by He_2^*) at time scales that are smaller than the breakdown time scale. While this was the case in Ref. 6, it is not immediately clear that this assumption holds for the plasma needle that is operated at a rf of 13.6 MHz. This will be discussed further in Sec. IV. Note that no radiative transitions were explicitly included in this approach: the energy necessary to produce radiative species was included as a loss term to the electron energy equation.

Recent measurements of the plasma needle¹² showed that typically there are nitrogen impurities present in the discharge gas. The impurity density is determined by the quality of the gas in the cylinder, as well as by diffusion of air into the active region of the discharge: close to the needle tip the gas can be expected to be most pure, while further away from the tip the impurity density increases. In the experiments, the amount of nitrogen in the center of the discharge was found to be below the detection limit of 0.5% of a Raman-scattering technique and was only detectable at a distance further away than approximately 1.5 mm from the tip of the needle. Considering that the plasma is most dense close to the needle, where the gas is most pure, we assumed that only helium is directly electronically excited and ionized. The excitation and ionization of N_2 are realized in heavy particle collisions only. For the calculations we used a uniform nitrogen fraction of 0.1% and disregarded the increase of impurities with a distance from the needle tip.

C. Needle geometry and circuit

We simplified the geometry of the plasma needle to a point-plane geometry with a cylindrical symmetry (see Fig. 2), defined on a rectangular grid of typically $N_z=100$ control

volumes in the axial direction and $N_r=100$ control volumes in the radial direction. The dimension of each control volume was $0.05 \times 0.05 \text{ mm}^2$.

In experimental practice, the discharge is part of a circuit that includes a rf source and a matching network. The matching network serves to adapt the impedance of the plasma to the output impedance of the power supply and thereby maximize transmission of power.¹⁷ It is outside the scope of the present paper to fully describe the nontrivial interaction between the plasma and the matching network. Instead, only one important feature was accounted for: no net current can run, due to a capacitor in series with the discharge. Before the discharge reaches steady state, any net current adds charge on the plates of the capacitor and will thereby contribute to a bias voltage that offsets the potential of the needle with respect to the earth potential. This bias voltage then counteracts the current and eventually reaches a steady-state level at which no net current runs. To simulate this, a single capacitor of 2 pF was modeled in series with the discharge. This relatively low value was chosen in order to minimize the time which it took for the simulation to reach steady state.

Although not experimentally ideal, it is possible to have a matching network with inductive instead of capacitive elements in series with the needle. In such a configuration a direct current can run. This was briefly investigated in order to study the interesting confining effect of the unbiased electrical potential on the electrons.

Finally, in experiments the helium gas flow through the Perspex tube surrounding the needle was typically in the order of 2 l/min. We neglected this flow because the directed velocity due to this flow was three orders of magnitude smaller than the thermal motion of the gas atoms.

III. RESULTS

The model described in Sec. II was used to investigate various aspects of the plasma needle. In the text that follows, we first look at the case in which the needle was placed at a distance of 3 mm from the plane and was driven by a voltage of 320 V in amplitude. This standard condition encompasses all characteristics of the needle that are also found at larger distances and yet there is no appreciable influence of the proximity of the plane. Following the study of this standard condition, we then examine the influence of parameters such as applied voltage and distance to the plane.

A. Discharge characteristics

In Fig. 3, the voltage applied to the needle and the periodic current running through the needle are shown for the standard condition ($V=320 \text{ V}$ and $d=3 \text{ mm}$). The steady-state bias voltage was -116 V and the dissipated power 31 mW. The total current lagged the voltage just a little less than $\pi/2$ rad, which indicates that the needle behaved almost completely capacitatively. This capacitive component is formed by the capacitance of the metal needle in its environment and gives rise to a displacement current. The discharge itself adds a small resistive component which is responsible for the dissipated power.

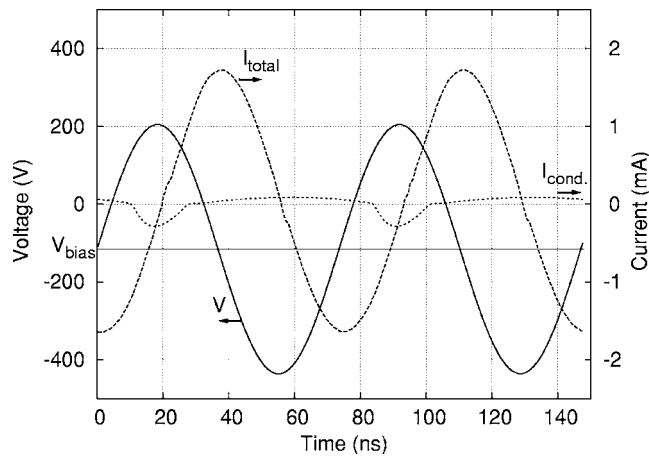


FIG. 3. The voltage, conduction current and total (i.e., conduction plus displacement) current as a function of time during steady-state operation of the needle for the standard conditions ($V=320$ V and $d=3$ mm). The horizontal line at -116 V indicates the bias voltage that offsets the needle potential with respect to earth.

Figure 4 shows the time-averaged electron-density profile. The maximum electron density was $3 \times 10^{11} \text{ cm}^{-3}$ and the size of the discharge, measured by the distance over which the electron density dropped by one order of magnitude, was in the order of 1 mm^3 . The electron energy close to the needle was calculated to be 8 eV and dropped quickly below 1.5 eV at a distance of 0.5 mm away from the needle.

Figure 4 shows that the plasma exhibited a large degree of spherical symmetry between the needle and the plane. In the following text we will therefore consider quantities at the axis of the discharge: these quantities show similar profiles along different lines at an angle from the needle towards the plane.

The axial, time-averaged densities profiles of the various species are depicted in Fig. 5. Of the species treated by the model, only N_2^+ and the electrons existed relatively far from the needle, while the other species were found within 0.4 mm of the needle tip. In this region close to the needle, the electric field was highest and the electron energy gained in this field was mainly lost in the production of He^* via

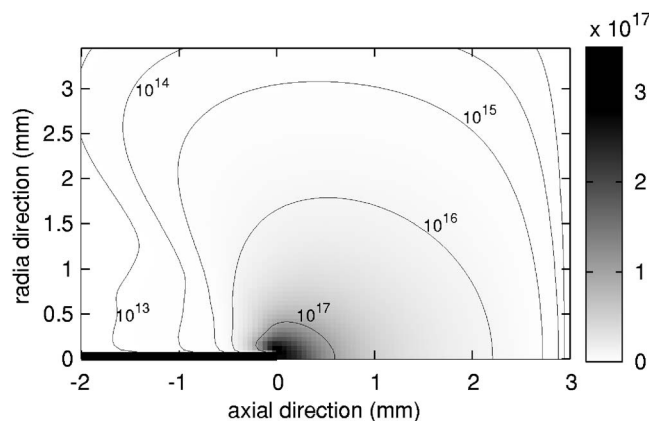


FIG. 4. The electron-density profiles, averaged over the rf cycle, for a needle at 3 mm from a plane, driven at 320 V . The contour lines show the density at a logarithmic scale, the different levels of gray show the density at a linear scale. Note that not the entire calculation domain is shown here.

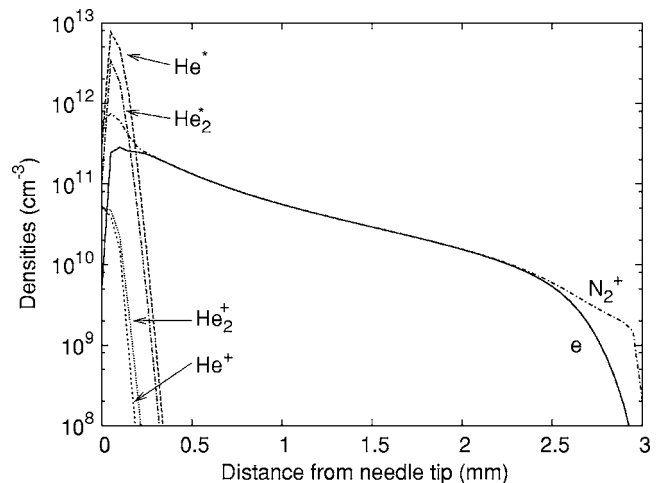


FIG. 5. The axial, time-averaged densities of the various species as a function of the distance to the needle tip. Most species existed only close to the needle and got rapidly converted in N_2^+ ions and electrons. These then diffused outward and recombined further away from the needle.

reaction 1 (in Table II). This energy, now contained in He^* , eventually resulted in the ionization of N_2 , either directly through Penning ionization in reaction 10 or via He_2^* (reactions 4 and 11). For the resulting N_2^+ ions, the destruction rate (reaction 13) was sufficiently low so that the main loss processes was that of ambipolar diffusion of this species outward, together with an equal number of electrons.

To give an impression on the time dependence of the reaction rates in the active region of the discharge, the rates are shown at a distance of 0.2 mm away from the tip of the needle in Fig. 6. Moving further away from the needle, all rates dropped to negligible values except for the rate of reaction 13.

The electron density and potential at the axis of the system are shown in Fig. 7 for different phases (0 , $\pi/2$, π , and $3\pi/2$ rad) during the rf cycle. The electron density oscillated with the rf cycle, with an amplitude of about 0.2 mm . Unlike the electrons, the spatial modulation of the ions was negli-

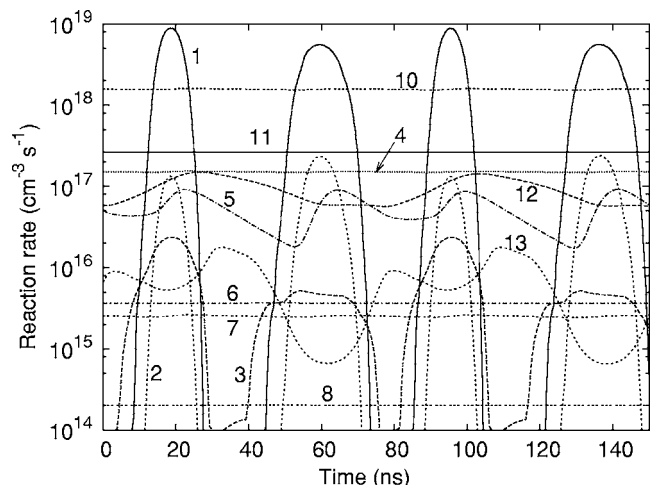


FIG. 6. The time-dependent reaction rates at a distance of 0.2 mm from the needle tip. The numbers near the curves correspond with the numbers in Table II. Refer to Fig. 3 for the phase of the applied voltage as a function of time.

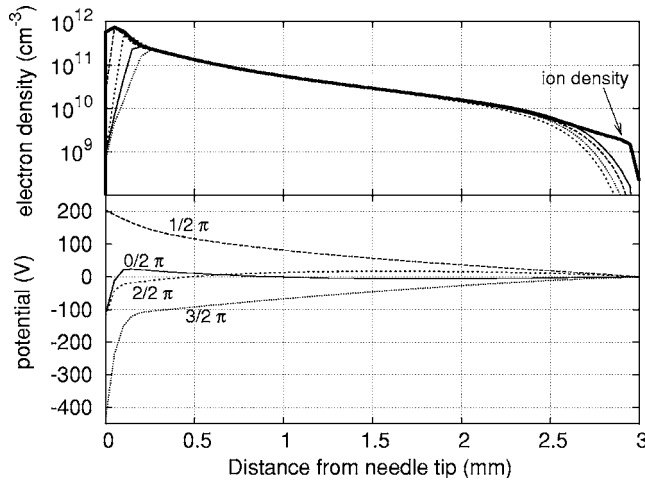


FIG. 7. The axial electron density and the potential at four different phases during the rf cycle. The bold continuous line in the top part of the graph shows the time-averaged ion density.

gible, due to their relatively large mass. The positive space-charge density that remained when the electrons moved away from the needle was responsible for the large cathode fall. During the anode phase, the space-charge density in front of the needle was small and did not contribute to the field appreciably.

B. Influence of distance and applied voltage

The applied voltage and distance of the needle to the plane are the control parameters that are normally important for the application of the needle. In order to investigate their influence on the dissipated power, these quantities were varied under otherwise equal conditions.

Figure 8 shows the effect of the applied voltage on the power. At higher powers, the maximum electron density was higher. Furthermore, the discharge became more elongated, that is, extended itself along the needle. The discharge thereby increased the extent of its sheath along the surface of the needle and could draw more current. This is consistent with experimental observations.

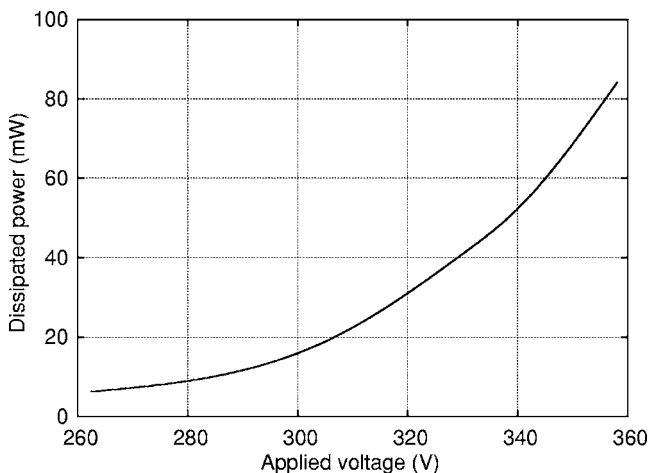


FIG. 8. The dissipated power as a function of the applied voltage for a distance of 3.0 mm between needle and plane.

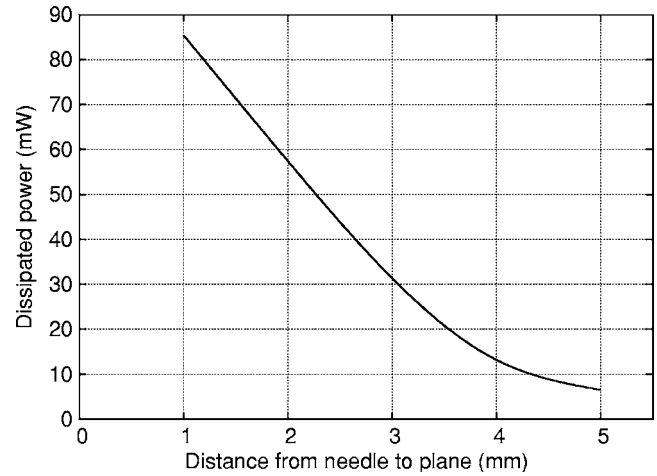


FIG. 9. The dissipated power as a function of the distance between needle and plane for an applied voltage of 320 V.

In Fig. 9 the effect of the distance between needle and plane is shown. For increasing distance, the magnitude of the field close to the needle decreased, which resulted in smaller dissipated powers.

C. Effect of current restriction

As mentioned in Sec. II, the matching network of the needle often contains a capacitor in series with the needle. Before the system reaches steady state, this capacitor generally accumulates charge and thereby introduces an offset in the average needle voltage that eventually prevents a net current from running. Instead of this configuration, it is feasible to make a matching network that contains only an inductance in series with the needle. In such a circuit, net currents do not lead to a bias voltage and this absence of bias voltage has a large effect on the steady-state field configuration.

In the unbiased situation, we found that the electric field was such that the electrons were confined to a region close to the needle, while the ions were not. Figure 10 shows the

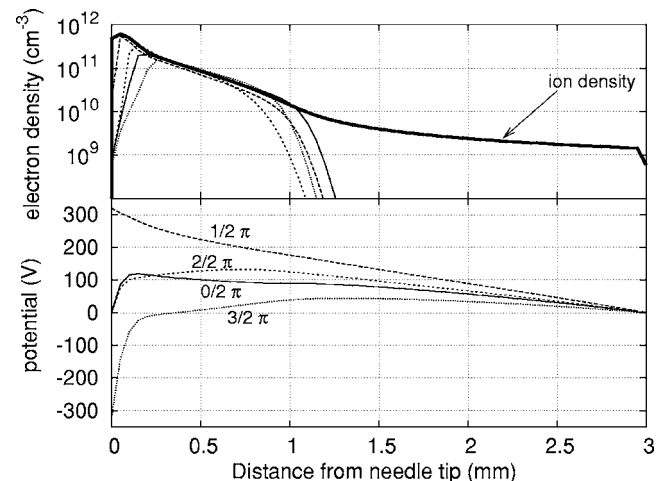


FIG. 10. The axial electron density and the potential at four different phases during the rf cycle for the situation in which the current is not restricted by a bias voltage across a capacitor. The bold continuous line in the top part of the graph shows the time-averaged ion density. Compare with Fig. 7 for the biased situation.

charged particle densities and potential for this case. One can see that the electrons did not move further away than approximately 1 mm from the tip of the needle. Beyond that distance the field pointed towards the needle during the entire rf cycle. The average potential at this distance corresponded to the absolute value of the bias voltage, as was observed in the simulation of which results are presented in Fig. 7.

This simulation also allowed us to obtain an estimate of the time scale for the discharge to reach steady state. We applied a 10% step in the voltage from $V=320$ V to $V=352$ V and looked at the time that it took for the power to reach its final value within a fraction of $1/e$ of the difference between the original and final values. This was $20 \mu\text{s}$. The equilibration time scale of the discharge is thus several times these $20 \mu\text{s}$.

In a circuit containing a capacitor, a second time scale is formed by the time at which the bias voltage sets itself. Given a current of typically $1 \mu\text{A}$ in the unbiased situation and a capacitor in the order of 10 pF , the relation $I = (CdV/dt)$ predicts a time scale in the order of 1 ms for a capacitor to charge and thus for steady state to settle.

IV. DISCUSSION

In the following paragraphs we will discuss the results presented in Sec. III in terms of consistency with experimental data and in terms of what important physical processes that underly them. Also, some assumptions are discussed that could not *a priori* be considered correct.

A. Comparison to experiments

In Sec. III, simulations for the standard condition ($V=320$ V and $d=3$ mm) predicted that the electron density is typically of the order of 10^{11} cm^{-3} . The size of the plasma is typically 1 mm. N_2^+ was the dominant ion, even for small admixtures of nitrogen. The power dissipated in the discharge ranged from 10 to 100 mW and was strongly dependent on both the applied rf voltage and the distance of the needle to the plane.

These results do agree with the experimental data that were available at the time of writing this paper: from the experiments¹⁰ we know that the amplitude of the voltage applied to the needle typically ranges from 200 to 350 V for a small, stable plasma; the (visually determined) size of the discharge is ~ 1 mm, the electron density is estimated to be $\sim 10^{11} \text{ cm}^{-3}$, and the dissipated power is in the order of 100 mW.

The most directly measured quantity was the dissipated power¹⁷ and therefore especially this quantity is a suitable parameter to compare the model with the experiments. Given the figures mentioned in Refs. 10 and 18, the results shown in Fig. 8 suggest that the calculated power dissipation at the above-mentioned voltage is at most a factor of 10 too low. However, it is not exactly known how much power is dissipated in the matching network and how this depends on the distance from the needle to plane. Due to this uncertainty, the measured power reported in Ref. 10 can be considered to be the upper limit of the power that is actually dissipated in the

plasma itself. In Ref. 18 powers are reported in the range of 0–50 mW, however, here the applied voltage to the needle is not given, which makes the figures reported in this paper unsuitable for direct comparison. In addition to the experimental uncertainties, a further reason for this discrepancy could be that in the model the electric field at the tip of the needle is underestimated due to a limited sharpness of the needle as a result of the coarseness of the numerical grid. A higher field results in a higher ionization rate and leads to higher electron densities and more power dissipation.

Therefore, although the measured and calculated values of the dissipated power differ, there are both experimental and computational factors which make agreement or disagreement uncertain. Further research will have to be done in order to make better conclusions on this subject.

B. Reaction kinetics

Various assumptions were made in constructing the set of reactions between the various species described by the model. The validity of several of these assumptions was treated in Sec. II. Here we discuss the others.

In the first place, we assumed that the various excimer levels of the helium molecular system decay into the $a^3\Sigma_u^+$ state over time scales that are faster than the rf period. In Fig. 6, the reaction rates are shown as a function of time in the rf cycle. Reaction number 4 is the reaction that treats the compound of reactions that eventually result in the $a^3\Sigma_u^+$ state. One can see in the figure that this reaction rate is not significantly modulated during the rf cycle. This indicates that the typical time scales involved here are longer than the rf time scale and that it is therefore reasonable to treat only this one excimer state.

Furthermore, note that in the experimental setup the gas is not uniform in its impurities: the helium flow along the needle ensures that the gas close to the needle is almost as pure as that contained in the source cylinder. Further away from the needle, the purity is decreased due to inward diffusion of air and perhaps molecules from a nearby surface. Since the active plasma is confined to a region close to the needle, this disuniformity further away from the needle will not effect the results significantly.

From the results presented in Sec. III it has become clear that only a small region close to the needle exhibits active production of species. Only N_2^+ ions and electrons can diffuse away from this region due to their relatively low recombination rates. One can consider the region close to the needle as a point source from which these species diffuse away radially with an ambipolar diffusion constant D_{amb} and are destroyed with a rate $S=kn_en_i$. After equating n_e to n_i and assuming the rate k of reaction 12 to be constant, the particle densities outside of the productions region can be described by the balance equation of n_e in spherical coordinates, for $r>0$,

$$\nabla^2 D_{\text{amb}} n_e(r) = \frac{D_{\text{amb}}}{r^2} \frac{d}{dr} r^2 \frac{d}{dr} n_e(r) = kn_e^2. \quad (3)$$

Solving this equation yields

$$n_e(r) = c \frac{2D_{\text{amb}}}{kr^2}, \quad (4)$$

where c is a constant that depends on the density of the electron-ion pairs at the border of the production region. The decrease in density as a function of r as predicted by this equation is slower than observed in, for example, Fig. 5. One reason for this could be that both D and k are taken to be constants, while, in fact, they are dependent on the electron temperature. Depending on the distribution and nature of pollutants, N_2 and the electrons might react to form negative ions and radicals further away from the needle tip.

These results suggest that in a future theoretical description of the needle, a distinction can be made between the production region close to the needle and a recombination region further away from the needle. A more advanced description could exploit this by modeling the former region in more detail with a denser grid and add the latter region by adding more impurities and corresponding reactions and take the complex interaction with biological materials into account. The coupling of the two regions can be described by the outward flux of N_2^+ and electrons.

C. Effect of current restriction

A few simulations were run in which no capacitor was assumed to be in series with the needle and, therefore, a net current could run. If a capacitor is connected in series with the needle (as is the case in most matching networks), such a net current charges the capacitor and offsets the average potential of the needle. When the bias voltage is not present, the average electric field is distinctly different from the biased situation and has its effect on the discharge. Although there is no experimental data on the behavior of the discharge in this situation, we included some numerical results that might point the way to future experiments.

If one compares Fig. 10 for the unbiased case with Fig. 7 for the biased case, one can see that the main effect of this different electric field is the confinement of electrons to a region close to the needle. Outside this region the current is carried by ions alone. A matching network based on an inductive element instead of a capacitor could accomplish this situation, perhaps offering a way to control the nature of the species arriving at a substrate.

Note that a similar situation also temporarily arises for a needle driven by a regular matching network when the steady-state bias voltage of the device is suddenly altered. This can, for example, happen when one of the experimental setting is suddenly changed, or when the electrical potential of the environment alters. The time it then takes for a new steady state to set depends on the net current and the capacitance of the matching network and was estimated to be in the order of 1 ms.

V. CONCLUSIONS

In this paper we presented a numerical description of the plasma needle. We used a two-dimensional, time-dependent fluid model and included a set of species and reactions that was designed earlier for a dielectric barrier discharge with

similar conditions. This set is on the one hand detailed enough to give a realistic model of the needle and on the other hand terse enough to be able to give insight in what the important processes are. With this model, the electrical properties of the needle and the spatiotemporal evolution of quantities such as particle densities could be predicted. These insights can help in explaining observations in present experiments and in giving direction to future experiments. More experimental data will be necessary to improve and further validate the model.

This study has shown that the electron density in the plasma is typically of the order of 10^{11} cm^{-3} . The size of the plasma, measured by the distance over which the electron density dropped by one order of magnitude, is typically 1 mm. Even at small admixtures of nitrogen, N_2^+ was found to be the dominant ion. The power dissipated in the discharge ranged from 10 to 100 mW and was strongly dependent on both the applied rf voltage and the distance of the needle to the plane. For higher powers the plasma covered more surface of the needle. These findings are consistent with the few experimental data available.

The simulations showed that the reaction kinetics are most important in the sheath and that the end products of the reactions were N_2^+ ions and electrons, which diffused from this region and recombined at some distance from the needle. Future models could exploit this fact by distinguishing between the production region and the recombination region. The former could be described by a finer numerical grid and use effluxes as boundary conditions for the balance equations. The latter could be refined by including more impurities and reaction, which originate from the inward diffusion of air and of species from the treated surface.

Finally, the design of the matching network could be used for controlling the charged species densities that diffuse away from the needle: if a dc is allowed to flow, the electrons are confined to a region close to the needle and only positive ions carry the current towards a surface.

ACKNOWLEDGMENT

We would like to acknowledge Philips Research for funding this investigation.

¹E. Stoffels, A. J. Flikweert, W. W. Stoffels, and G. M. W. Kroesen, *Plasma Sources Sci. Technol.* **11**, 383 (2002).

²J. van Dijk, Y. Horiuchi, and T. Makabe, *Bull. Am. Phys. Soc.* **48**, 17 (2003).

³I. E. Kieft, J. L. V. Broers, V. Caubet-Hilloutou, D. W. Slaaf, F. C. Ramaekers, and E. Stoffels, *Bioelectromagnetics (N.Y.)* **25**, 362 (2004).

⁴E. A. Sosnin, E. Stoffels, M. V. Erofeev, I. E. Kieft, and S. E. Kunts, *IEEE Trans. Plasma Sci.* **32**, 1544 (2004).

⁵J. Park, I. Hennins, H. W. Herrmann, and G. S. Selwyn, *J. Appl. Phys.* **89**, 20 (2001).

⁶Yu. B. Golubovskii, V. A. Maiorov, J. Behnke, and J. F. Behnke, *J. Phys. D* **36**, 39 (2003).

⁷L. Mangolini, C. Anderson, J. Heberlein, and U. Kortshagen, *J. Phys. D* **37**, 1021 (2004).

⁸G. J. M. Hagelaar, M. H. Klein, R. J. M. M. Snijkers, and G. M. W. Kroesen, *J. Appl. Phys.* **89**, 2033 (2001).

⁹W. J. M. Brok, J. van Dijk, M. D. Bowden, J. J. A. M. van der Mullen, and G. M. W. Kroesen, *J. Phys. D* **36**, 1967 (2003).

¹⁰I. E. Kieft, E. P. van der Laan, and E. Stoffels, *New J. Phys.* **6**, 149 (2004).

¹¹BOLSIG, Boltzmann solver for the siglo-series 1.0. CPA Toulouse & Kinema Software, 1996.

- ¹²I. E. Kieft, J. J. B. N. van Berkel, E. R. Kieft, and E. Stoffels, Special issue of Plasma Processes and Polymers **2**, 295–308 (2005).
- ¹³E. W. McDaniel, *Collision Phenomena in Ionized Gases* (Wiley, New York, 1964).
- ¹⁴*Handbook of Physical Quantities*, edited by I. S. Grigoriev and E. Z. Meilikhov (CRC, Boca Raton, FL, 1997).
- ¹⁵H. W. Ellis, R. Y. Pai, E. W. McDaniel, E. A. Mason, and L. A. Viehland, At. Data Nucl. Data Tables **17**, 177 (1976).
- ¹⁶R. K. Janev, W. D. Langer, D. E. Post, Jr., and K. Evans, Jr., *Elementary Processes in Hydrogen-Helium Plasmas* (Springer, Berlin, 1985).
- ¹⁷Yu. P. Raizer, M. N. Shneider, and N. A. Yatsenko, *Radio-Frequency Capacitive Discharges* (CRC, Boca Raton, FL, 1995).
- ¹⁸E. Stoffels, R. E. J. Sladek, I. E. Kieft, H. Kersten, and R. Wiese, Plasma Phys. Controlled Fusion **46**, B167 (2004).

Journal of Applied Physics is copyrighted by the American Institute of Physics (AIP). Redistribution of journal material is subject to the AIP online journal license and/or AIP copyright. For more information, see <http://ojps.aip.org/japo/japcr/jsp>